Acta Crystallographica Section D
Biological Crystallography
ISSN 0907-4449

Structural insights into the adaptation of proliferating cell nuclear antigen (PCNA) from *Haloferax volcanii* to a high-salt environment

Ekaterina Morgunova,[a]* Fiona C. Gray,[b] Stuart A. MacNeill[b,c] and Rudolf Ladenstein[a]

[a]Karolinska Institutet, NOVUM, Centre of Structural Biochemistry, S-14157 Huddinge, Sweden, [b]Department of Biology, University of Copenhagen, Ole Maaløes Vej 5, 2200 Copenhagen, Denmark, and [c]Centre for Biomolecular Sciences, University of St Andrews, North Haugh, St Andrews, Fife KY16 9ST, Scotland

Correspondence e-mail: ekaterina.morgunova@ki.se

Received 19 May 2009
Accepted 23 July 2009

PDB Reference: proliferating cell nuclear antigen, 3hi8, r3hi8sf.

The sliding clamp proliferating cell nuclear antigen (PCNA) plays vital roles in many aspects of DNA replication and repair in eukaryotic cells and in archaea. Realising the full potential of archaea as a model for PCNA function requires a combination of biochemical and genetic approaches. In order to provide a platform for subsequent reverse genetic analysis, PCNA from the halophilic archaeon *Haloferax volcanii* was subjected to crystallographic analysis. The gene was cloned and expressed in *Escherichia coli* and the protein was purified by affinity chromatography and crystallized by the vapour-diffusion technique. The structure was determined by molecular replacement and refined at 3.5 Å resolution to a final R factor of 23.7% ($R_{\rm free}$ = 25%). PCNA from *H. volcanii* was found to be homotrimeric and to resemble other homotrimeric PCNA clamps but with several differences that appear to be associated with adaptation of the protein to the high intracellular salt concentrations found in *H. volcanii* cells.

1. Introduction

Proliferating cell nuclear antigen (PCNA), also known as a sliding clamp, plays vital roles in many aspects of DNA replication, repair and recombination in eukaryotic and archaeal cells (Johnson & O'Donnell, 2005). PCNA is a trimeric ringed-shaped oligomer that encircles double-stranded DNA (dsDNA), along which it can freely slide. The loading of PCNA onto DNA requires that the ring is first opened and then re-closed in an ATP-dependent reaction catalysed by the replication factor C (RFC) complex. When loaded onto dsDNA, PCNA acts as a platform on which other protein factors assemble. Many of these proteins interact with PCNA *via* a short peptide sequence (called the PCNA-interacting protein peptide or PIP peptide) that binds tightly to a hydrophobic pocket on the surface of the PCNA trimer (Warbrick, 1998). These interactions are conserved in both eukaryotic and archaeal systems (Johnson & O'Donnell, 2005).

Structures of eukaryotic PCNA complexes have been determined for the budding yeast *Saccharomyces cerevisiae* (Krishna *et al.*, 1994) and human (Gulbis *et al.*, 1996; Kontopidis *et al.*, 2005). In each case, the structures revealed a pseudo sixfold-symmetrical architecture with each PCNA monomer comprising two topologically identical domains. The central cavity of the ring, through which the dsDNA passes, is predominantly positively charged. Additional available structures show the interactions of yeast PCNA with the pentameric RFC complex (Bowman *et al.*, 2004), as well as

with the PIP peptide derived from the DNA ligase I protein Cdc9 (Vijayakumar *et al.*, 2007), and the interactions of human PCNA with PIP peptides derived from DNA polymerases δ, η, ι and κ (Bruning & Shamoo, 2004; Hishiki *et al.*, 2009), the DNA-replication and cell-cycle inhibitor $p21^{Cip1}$ (Gulbis *et al.*, 1996) and the nuclease Fen1 (Bruning & Shamoo, 2004; Sakurai *et al.*, 2005).

The archaeal chromosomal DNA replication machinery resembles a simplified form of that found in eukaryotic cells and has attracted attention as a model system for studying the processes of DNA replication at the molecular level (Grabowski & Kelman, 2003). Archaeal PCNA complexes have also been identified and subjected to extensive biochemical and structural analysis. Crystal structures have been obtained for the homotrimeric PCNA complexes of the euryarchaeal species *Archaeoglobus fulgidus* (Chapados *et al.*, 2004) and *Pyrococcus furiosus* (Matsumiya *et al.*, 2001, 2002) as well as for the heterotrimeric PCNA from the crenarchaeal species *Sulfolobus solfataricus* (Williams *et al.*, 2006). PIP peptide-bound structures are also available for *A. fulgidus* and *P. furiosus* PCNAs bound to PIP peptides derived from Fen1 and RFC, respectively (Chapados *et al.*, 2004; Matsumiya *et al.*, 2002), and for *S. solfataricus* PCNA bound to PIP peptides from Fen1 (Williams *et al.*, 2006) and the translesion DNA polymerase Dpo4 (Xing *et al.*, 2009).

Realising the full potential of archaea as a model for PCNA function requires a coupling of biochemical and genetic approaches, yet this is hindered by the fact that the majority of well studied archaeal organisms are refractive to genetic analysis (Allers & Mevarech, 2005). However, this is not the case for several of the halophilic euryarchaea, such as *Haloferax volcanii*. This organism, which was first isolated in the Dead Sea, is an obligate halophile that grows optimally under aerobic conditions at 318 K in a medium containing 20% NaCl (Mullakhanbhai & Larsen, 1975). Under these conditions, the internal KCl concentration of the cells has been measured as 3–4 *M* (reviewed in Muller & Oren, 2003). A wide range of materials and methods for genetic manipulation of *H. volcanii* have been described, including an efficient transformation system, plasmid vectors, selectable and counter-selectable markers, constitutive and regulatable promoters and reporter genes (reviewed in Allers & Mevarech, 2005).

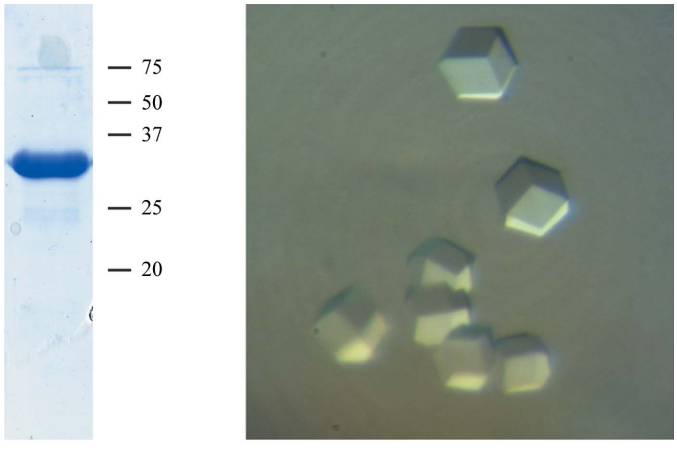

(*a*) (*b*)

Figure 1
(*a*) Purified recombinant *Hfx*PCNA (5 µg) visualized by PAGE Blue 90 staining following SDS–PAGE. The positions of molecular-weight markers (in kDa) are shown to the right. (*b*) Crystals of *Hfx*PCNA belonging to monoclinic space group *C*2, with unit-cell parameters a = 174.4, b = 123.2, c = 123.3 Å, α = 90, β = 135, γ = 90°.

Table 1
Data-collection and refinement statistics.

Values in parentheses are for the highest resolution shell.

Data collection	
Resolution limits (Å)	30–3.5 (3.65–3.5)
No. of observed reflections	1454357
No. of unique reflections	26380
Completeness (%)	99.3 (86.3)
Average redundancy	3.9 (3.8)
$I/\sigma(I)$	8.6 (2.6)
R_{merge}† (%)	9.8 (57.7)
Wilson B factor (Å^2)	125.1
Refinement	
No. of non-H protein atoms	11214
No. of solvent molecules	31
Resolution range (Å)	30.0–3.5
R_{cryst}‡ (%)	23.7
R_{free}§ (%)	25.0
Ramachandran plot	
Most favourable regions (%)	80.5
Additional allowed regions (%)	18.6
Generously allowed regions (%)	0.0
Disallowed regions (%)	0.9
R.m.s. standard deviation	
Bond lengths (Å)	0.01
Bond angles (°)	1.49
Average B factor/SD (Å^2)	139.4

† $R_{merge} = \sum_{hkl}\sum_i |I_i(hkl) - \langle I(hkl)\rangle| / \sum_{hkl}\sum_i I_i(hkl)$, where $I_i(hkl)$ is the scaled intensity of the ith observation of reflection hkl and $\langle I(hkl)\rangle$ is the mean intensity for that reflection. ‡ $R_{cryst} = \sum_{hkl} ||F_{obs}| - |F_{calc}|| / \sum_{hkl} |F_{obs}|$. § R_{free} is the cross-validation R factor computed for a test set of 5% of the unique reflections.

Recently, we initiated a reverse genetic analysis of *H. volcanii* PCNA (*Hfx*PCNA) in order to allow us to probe questions of protein structure and function in living archaeal cells (unpublished results). Rather than rely on the structures of PCNA complexes from the hyperthermophilic species *P. furiosus* and *A. fulgidus* to guide our mutational analysis, we subjected *Hfx*PCNA to structure determination by X-ray crystallography. In the present report, we describe the three-dimensional structure of PCNA from *H. volcanii* at 3.5 Å resolution, compare it with orthologues from different organisms and consider how this protein has adapted to its natural high-salt environment.

2. Material and methods

2.1. Gene cloning, expression and purification of *Hfx*PCNA

The PCNA ORF was amplified by PCR from genomic DNA prepared from *H. volcanii* strain DS70 (Wendoloski *et al.*, 2001) using the following oligonucleotide primers: HFXPCNA-5SAN (5′-GGTTGGTTGG**GGGACCC**GGG-ATGTTCAAGGCCATC-3′) and HFXPCNA-3BAM (5′-GGTGGTGGTT**GGATCC**TCAGTCGCTCTGGATGCG-3′). The PCR product was digested with the restriction enzymes

*San*DI and *Bam*HI (sites shown in bold in the oligonucleotide sequences) and cloned into plasmid pET47b (Novagen) that had previously been digested with the same two enzymes so that the 247-amino-acid PCNA protein could be expressed as a fusion protein with a 20-amino-acid N-terminal sequence that included a hexahistidine tag (MAHHHHHHSAAELV-LFQGPG). Expression was carried out in *Escherichia coli* Rosetta 2 (DE3) [pLysS] cells (Novagen). 1 l cultures were grown to mid-exponential phase (OD = 0.8) at 310 K and chilled on ice for 10 min before expression was induced by the addition of IPTG to 1 m*M*. Growth was continued for 18 h at 293 K, after which the cells were harvested by centrifugation, resuspended in lysis buffer (20 m*M* NaH_2PO_4, 20 m*M* imidazole, 2.0 *M* KCl pH 8.0) and lysed by sonication. Cleared extracts were then subjected to affinity chromatography using Ni–NTA agarose (GE Healthcare) at room temperature. Following extensive washing with lysis buffer, bound *Hfx*PCNA was eluted in 20 m*M* NaH_2PO_4, 500 m*M* imidazole, 2.0 *M* KCl pH 8.0. Peak fractions were pooled and dialysed against 20 m*M* NaH_2PO_4, 20 m*M* imidazole, 2.0 *M* KCl pH 8.0 (Fig. 1*a*).

2.2. Crystallization and data collection

The concentrated protein was crystallized by the sitting-drop vapour-diffusion method at 293 K. Crystallization conditions were searched for using Hampton Research screening kits. Each droplet was made by mixing 1 µl reservoir solution with 1 µl protein solution, which was at a concentration of 4 mg ml^{-1} in 20 m*M* NaH_2PO_4 pH 8 containing 2 *M* potassium chloride and 20 m*M* imidazole. Crystals of cubic shape suitable for X-ray analysis were obtained using two different crystallization conditions: 1.6 *M* sodium citrate and 4 *M* sodium malonate. Both salt solutions were saturated, which fitted with the halophilicity of the investigated protein. Thus, neither different buffers nor additives could be used in order to improve the quality of the crystals. Cubic-shaped crystals grew in one month to a size of 0.15 mm only (Fig. 1*b*). Further attempts to find different crystallization conditions were not successful. Unfortunately, the slightly larger crystals obtained using sodium citrate were not suitable for deep freezing; thus, we were forced to use the smaller crystals grown in sodium malonate for data collection at 100 K. The crystals appeared to be single; however, X-ray exposure of these crystals and data processing revealed twinned lattices from their diffraction images.

A diffraction data set was collected from a single crystal at a temperature of around 100 K on beamline ID23-2 at the European Synchrotron Research Facility (ESRF; Grenoble, France) using the sodium malonate reservoir solution as a cryoprotectant. Statistics of data collection are presented in Table 1.

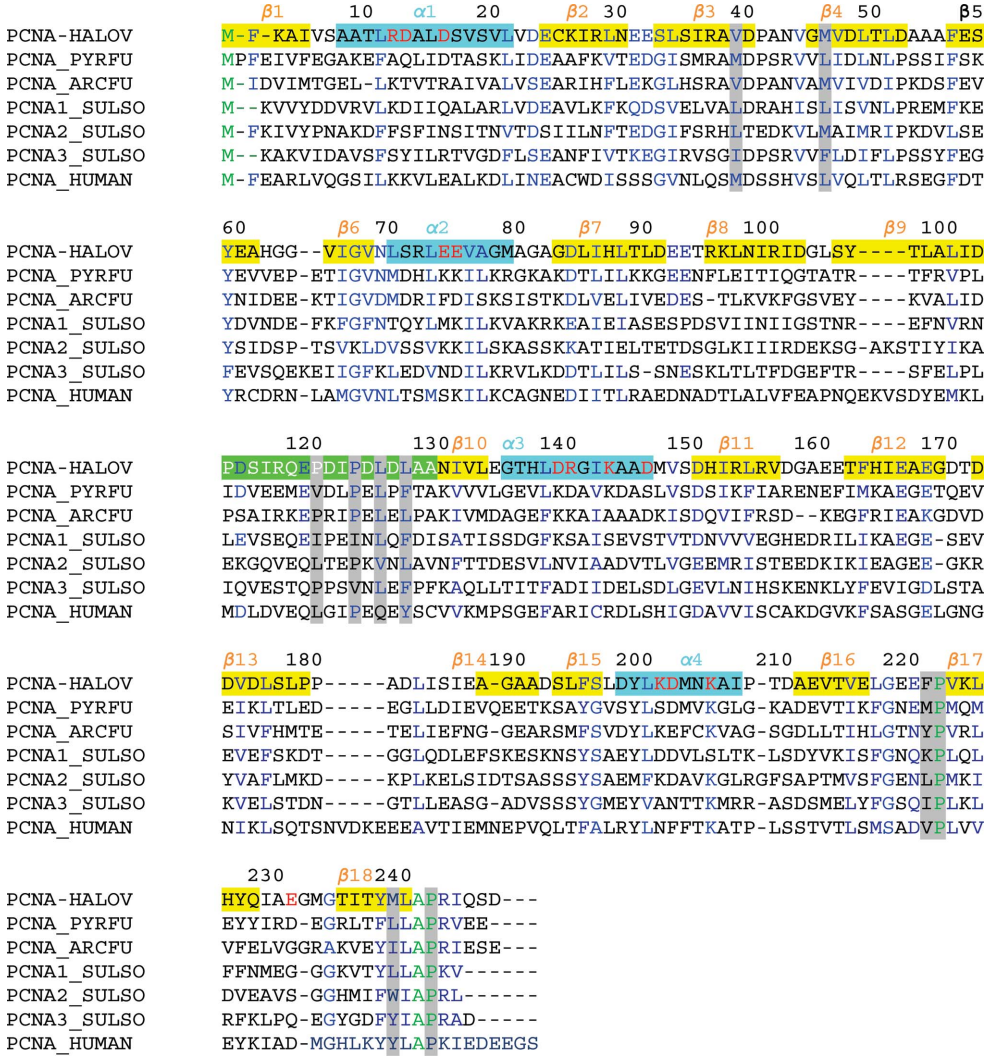

Figure 2
Sequence alignment of PCNAs from *H. volcanii* (PCNA_HALOV), *P. furiosus* (PCNA_PYRFU), *A. fulgidus* (PCNA_ARCFU), *S. solfataricus* (PCNA1_SULSO, PCNA2_SULSO, PCNA3_SULSO) and human (PCNA_HUMAN). The secondary-structure elements are shown above and labelled as they are found in the *Hfx*PCNA structure; α-helices are shown in cyan, β-strands are shown in yellow and the loop connecting the N-terminal and C-terminal domains is highlighted in green. Identical residues are coloured green, homologous residues are coloured blue, the positively/negatively charged residues which are unique to *Hfx*PCNA are coloured red and the residues that can be involved in PIP peptide interactions are highlighted in light grey.

2.3. Processing of the diffraction data and detection of twinning

The diffraction data were processed with the *HKL*-2000 package (Otwinowski & Minor, 1997). Auto-indexing of the diffraction data suggested six different lattices ranging from *C*-centred monoclinic to body-centred cubic, with a distortion index of between 0.89 and 2.98%. For comparison, all other lattices in the list showed a distortion index of greater than 14%. Initial processing of the data in space groups *C*2, *F*222, *I*222, *I*422, *R*32 and *I*23 showed a very similar $R_{\rm merge}$ of around 11%. Examination of the distribution of the intensities $\langle|I|^2\rangle/(\langle|I|\rangle)^2$ and the structure-factor amplitudes $(\langle|F|\rangle)^2/\langle|F|^2\rangle$ given by the program *TRUNCATE* from the *CCP*4 package (Collaborative Computational Project, Number 4, 1994) showed that the crystals were almost perfect pseudo-merohedral twins. This conclusion was confirmed by a twinning test run on the merohedral twinning server of the NIH MBI Laboratory (Yeates, 1997) and the *phenix.xtriage* routine from the program *PHENIX* (Adams *et al.*, 2002). The twin law and twinning fraction were determined by *phenix.xtriage* to be $h, -k, -h - l$ and 0.46, respectively. Close inspection of the systematic extinctions, the Laue symmetry of the diffraction pattern and a self-rotation function calculated in space group *P*1 suggested that the crystals can be characterized by unit-cell parameters $a = 174.4$, $b = 123.2$, $c = 123.3$ Å, $\alpha = \gamma = 90$, $\beta = 135^\circ$ and the symmetry of the monoclinic space group *C*2, which is a subgroup of the higher symmetry space groups observed in the initial processing. The calculated Matthews coefficient in space group *C*2 had a value of 2.42 Å^3 Da^{-1}, which corresponds to the presence of six protein molecules with a molecular weight of 28 kDa in the asymmetric unit.

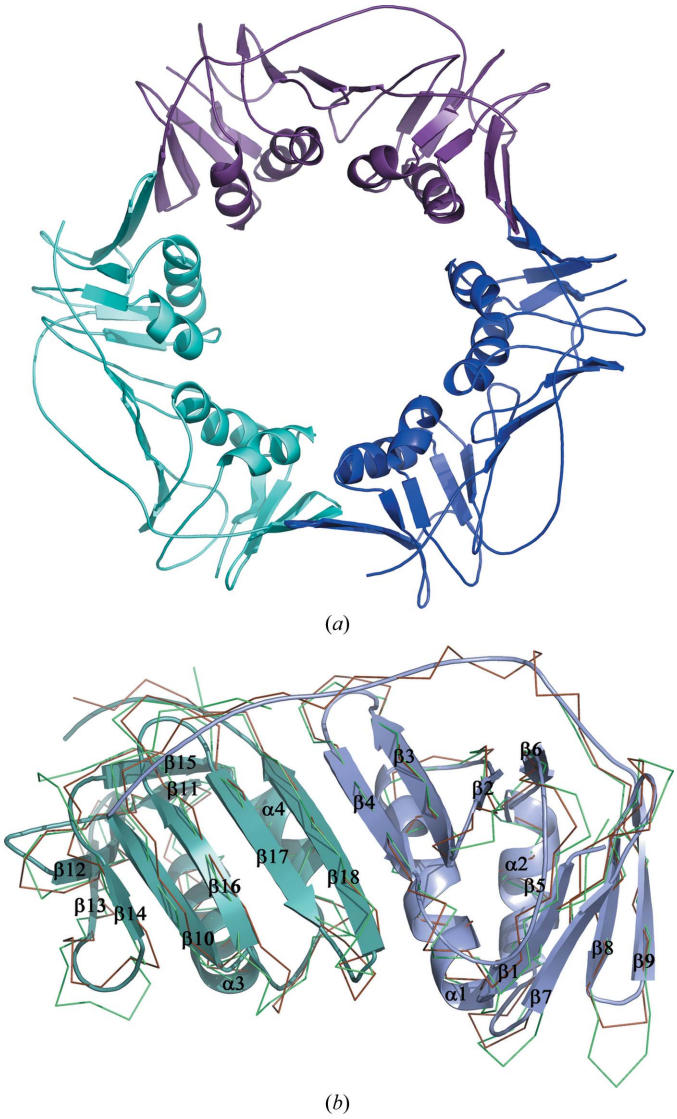

Figure 3
Structure of PCNA from *H. volcanii* (*Hfx*PCNA). (*a*) Homotrimer; three subunits are shown in different colours. (*b*) Ribbon representation of monomeric *Hfx*PCNA superimposed with PCNAs from *A. fulgidus* (brown; PDB code 1rwz; Chapados *et al.*, 2004) and *P. furiosus* (green; PDB code 1ge8; Matsumiya *et al.*, 2001). The N-terminal domain of *Hfx*PCNA is shown in blue and the C-terminal domain is shown in cyan; secondary-structure elements are assigned and labelled with respect to the *Hfx*PCNA structure. Figs. 3, 4 and 5 were generated with *PyMOL* (DeLano, 2002).

2.4. Structure solution and crystallographic refinement

Initial molecular-replacement trials were attempted in all suggested space groups using the program *MOLREP* as implemented in *CCP*4 (Collaborative Computational Project, Number 4, 1994), with the monomer structure of PCNA from *A. fulgidus* (PDB code 1rwz) as a Patterson search model. A sequence alignment performed with *ClustalW* (Thompson *et al.*, 1994) revealed a sequence identity of 37%, which appeared to be the highest percentage of identical residues between *Hfx*PCNA and all other known PCNA structures (Fig. 2). A correct molecular-replacement solution was only obtained in the monoclinic space group *C*2, in which six protein monomers in the asymmetric unit were found in individual searches one by one. Hence, the apparent monoclinic crystal lattice was confirmed.

2.4.1. Refinement. The crystallographic refinement was performed by *phenix.refine* (Adams *et al.*, 2002), first using a rigid-body refinement protocol with six rigid groups and then using the maximum-likelihood target with respect to the twinning operator determined as described above. Bulk-solvent correction and noncrystallographic restraints between six protein subunits were applied throughout refinement. The procedure improved the initial electron-density map and allowed the building of almost all of the residues that had been replaced by alanine in the original model. The model was rebuilt with the graphics programs *O* (Jones *et al.*, 1991) and *Coot* (Emsley & Cowtan, 2004). The progress of refinement was monitored by the free *R* factor, with 5% (1323 reflections) of the data put aside from the calculations. Several water molecules were built into the difference electron-density map at a late stage of refinement using *Coot*. The final model consisting of six protein subunits and 31 water molecules was refined at a resolution of 3.5 Å to an $R_{\rm cryst}$ of 23.7% and an $R_{\rm free}$ of 25%. The final refinement statistics are given in Table 1. The atomic coordinates and structure factors of

PCNA from *H. volcanii* have been deposited in the Protein Data Bank (entry 3hi8).

3. Results and discussion

3.1. Overall structure of PCNA from *H. volcanii*

PCNA from *H. volcanii*, in common with all other known PCNA orthologues, is organized in a characteristic toroidal structure (Fig. 3*a*) made up by three equivalent monomers. Every monomer in the ring interacts with two others in a head-to-tail manner. Thus, the six monomers found in the *C*2 asymmetric unit were organized into two separate rings. Each PCNA monomer contains 247 amino acids comprising two domains which are structurally duplicated and are connected to each other by long interdomain-connector loops (residues 116–128; Fig. 3*b*). The association of three monomers in the ring has apparent threefold noncrystallographic symmetry and the presence of two symmetrical domains in every monomer gives the trimer a pseudo sixfold-symmetrical appearance.

Each monomer domain consists of a nine-stranded β-sheet at one side and two α-helices at the other side. The middle β-strand (β4) interacts with the neighbouring β-strand (β18) from another domain by the formation of several hydrogen bonds. Thus, topologically the *Hfx*PCNA monomer belongs to the family of α/β proteins and is composed of an 18-stranded antiparallel twisted β-sheet and four α-helices (Fig. 3*b*). The helices of all three monomers are located inside the ring, whereas the extended β-sheet and connector loop form the outside surface of the ring.

The intersubunit contacts in the *Hfx*PCNA trimer are formed by strand β9 and helix α2 of one subunit and strand β13 and helix α3 of the neighbouring subunit. Six main-chain amide-to-carbonyl hydrogen bonds are formed between antiparallel strands β9 (residues 103–109) and β13 (residues 171–177) and one hydrogen bond is found between the side chains of Tyr106 and Asp172. The α-helices provide hydrophobic interaction patches that are formed by Val76 and Met79 from one subunit and Met147 and Ala144 from another subunit. Despite the low sequence homology, this type of subunit interaction is well conserved among all known PCNA structures.

Many of the proteins that interact with PCNA in both archaeal and eukaryotic cells do so *via* an evolutionarily conserved peptide sequence known as the PIP peptide (Warbrick, 1998). In haloarchaeal cells, proteins containing PIP peptides include the DNA polymerases PolB and PolD, the large subunit of replication factor C and the nucleases Fen1 and Rnh2 (see Fig. 2 in MacNeill, 2009). In each of these, the PIP peptide is located at the extreme C-terminus of the protein. Structural analyses have shown that the PIP peptide binds tightly in a hydrophobic pocket on the surface of PCNA that is predominantly composed of residues from the PCNA interdomain-connector loop (IDCL) but which also involves the hydrophobic side chains of residues located towards the N- and C-termini of PCNA (Gulbis *et al.*, 1996; Matsumiya *et al.*, 2002; Chapados *et al.*, 2004). Mutation of these residues results in impaired binding to the PIP peptide sequence. The residues that form this binding site in *Hfx*PCNA are almost identical to those of other archaeal PCNA molecules. For example, eight of ten hydrophobic residues (Val39, Met41, Pro120, Pro123, Leu125, Leu127, Pro220 and Pro240) identified as being involved in *A. fulgidus* PCNA–FEN-1 interactions (Chapados *et al.*, 2004) are identical in the *Hfx*PCNA protein sequence (Fig. 2) and form a similar hydrophobic pocket in three dimensions (Fig. 4). The ninth and tenth residues implicated in formation of the *A. fulgidus* PCNA pocket, Tyr219 and Leu239, are replaced by Phe221 and Met239 in *Hfx*PCNA, respectively (Figs. 2 and 4). Taken together, these observations indicate that the mode of PCNA–PIP peptide binding observed in mesohalic thermophilic archaeal organisms such as *A. fulgidus* is likely to be conserved in halophiles such as *H. volcanii*, but confirmation of this will require cocrystallization of a haloarchaeal PCNA with a cognate PIP peptide.

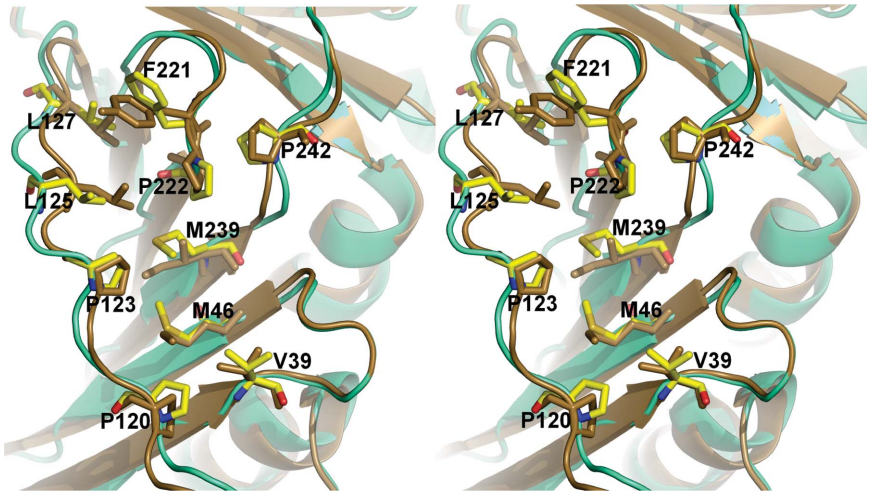

Figure 4
Stereoview of a structural comparison of PIP peptide-binding sites in *Hfx*PCNA (shown in cyan) and PCNA from *A. fulgidus* (shown in brown; PDB code 1rwz; Chapados *et al.*, 2004) showing conserved hydrophobic side chains. The residues involved in the binding sites are represented by sticks.

3.2. Structural comparison of HfxPCNA and charge distribution on the surface

The structural comparison of *Hfx*PCNA with archaeal orthologues from *P. furiosus*, *A. fulgidus* and three different PCNAs from *S. solfataricus* showed a very similar arrangement in homotrimers, with r.m.s.d. values of 1.6, 1.3, 2.6, 2.1 and 2.2 Å, respectively. The overlaid structures of monomers from the same organisms revealed a very similar arrangement in the central β-sheet; however, the flanking helices α2 and α3 are slightly shifted in the compared structures. The loops connecting secondary-structure elements are the most different parts in terms of length and con-

formation. Thus, in the N-terminal domain of *Hfx*PCNA the loops 61–64, 80–83 and 101–103 are the shortest among the archaeal structures known so far, whereas the C-domain loops of *Hfx*PCNA are the longest and have rather different conformations compared with the other orthologues. It is apparent from the r.m.s. deviation between different PCNAs that the protein from *A. fulgidus* is the closest structural homologue to *Hfx*PCNA. The sequence alignment reveals a very low homology even among archaeal organisms; however, sequence analysis with the *ProtParam* tool (Gasteiger *et al.*,

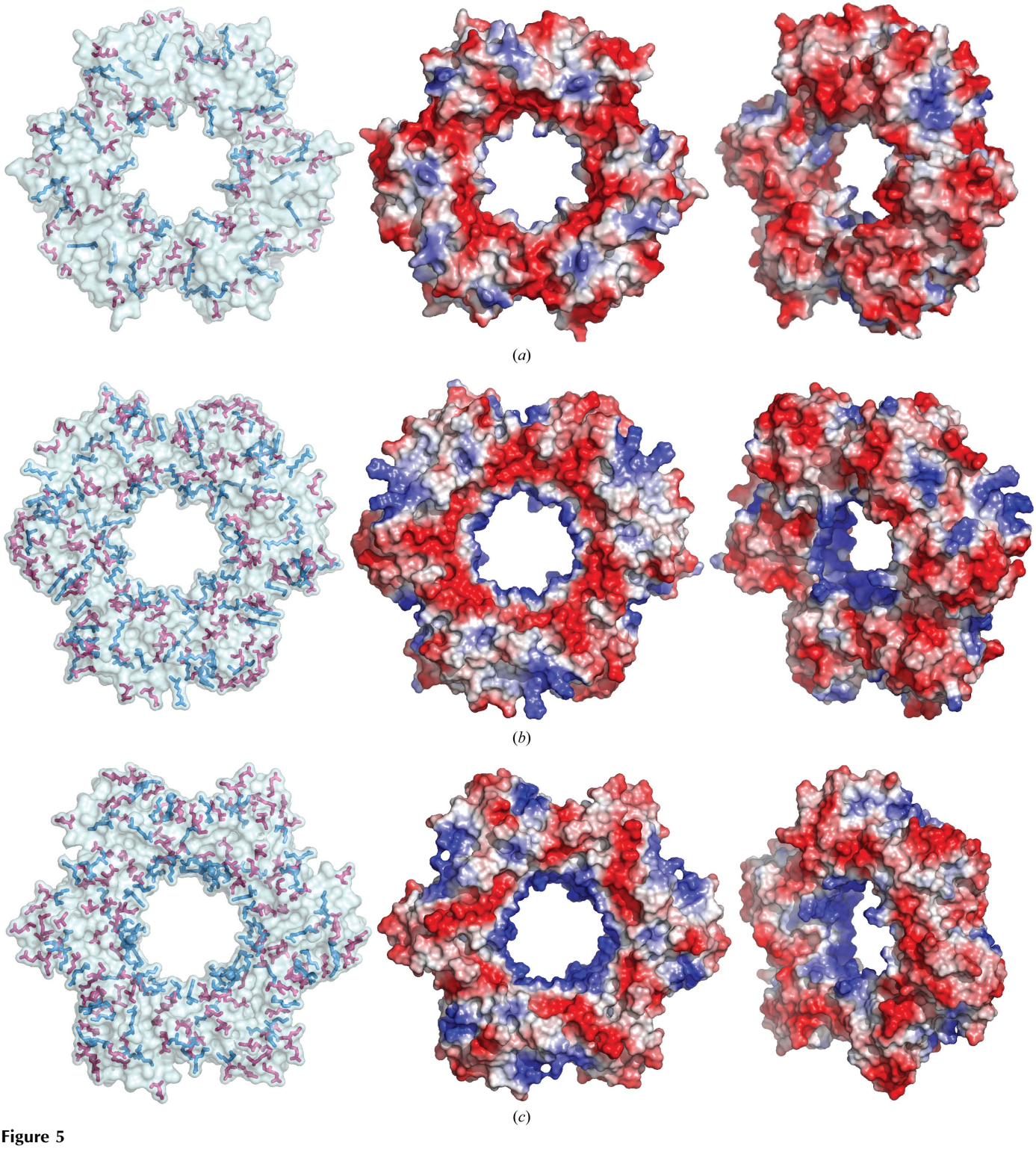

Figure 5
The distribution of negatively and positively charged residues on the surface of PCNA from (*a*) *H. volcanii*, (*b*) *A. fulgidus* (PDB code 1rwz; Chapados *et al.*, 2004) and (*c*) *P. furiosus* (PDB code 1ge8; Matsumiya *et al.*, 2001) and respective electrostatic potential maps in two different orientations. Residues are represented by sticks. Lysines/arginines are shown in blue and aspartates/glutamates are shown in red.

2005) showed a high level of positively and negatively charged surface residues, which is known to be a characteristic of extremophilic proteins (Karshikoff & Ladenstein, 2001). *Hfx*PCNA, which is the first representative of a halophilic PCNA, showed many fewer positively charged residues (seven lysines and 11 arginines in *Hfx*PCNA compared with 19 lysines and 12 arginines in *A. fulgidus* PCNA and 21 lysines and nine arginines in *P. furiosus* PCNA; Fig. 5*a*) but a similar fraction of negatively charged aspartate and glutamate residues (28 aspartates and 21 glutamates in *Hfx*PCNA compared with 19 aspartates and 25 glutamates in *A. fulgidus* PCNA and 17 aspartates and 33 glutamates in *P. furiosus* PCNA). A structural visualization of the charges on the surfaces of *P. furiosus* and *A. fulgidus* PCNA showed a rather typical distribution of positive and negative residues (Figs. 5*b* and 5*c*). The strong positive charge arising from several lysines and arginines is known to be responsible for the interaction with DNA and is located on the inner surface of the trimeric channel. Additional positively charged residues are equally distributed on the surface and are compensated by the negative charges from Asp and Glu residues. In contrast to the description given above, the structure of *Hfx*PCNA showed a relatively weak positive charge inside the channel (only three lysines and two arginines compared with 11 lysines and one arginine in *P. furiosus* PCNA and seven lysines and one arginine in *A. fulgidus* PCNA). The negative charges formed by 22 Asp and 18 Glu residues are randomly distributed on the surface and cannot be compensated by the nine Arg and four Lys residues that are also found on the surface (Fig. 5*a*). The most notable feature of protein halophilicity is the presence of clusters of non-interacting negatively charged surface residues. Thus, the distribution found in *Hfx*PCNA is consistent with this feature. Such negatively charged clusters are associated with unfavourable electrostatic energy at low salt concentration and may account for the instability of the protein at a salt concentration lower than 2.5 *M*. The central channel in *Hfx*PCNA contains only three lysine residues (Lys143, Lys201 and Lys205) and two arginine residues (Arg12 and Arg140) and thus is much less positively charged in comparison to all archaeal and previously determined PCNA structures. Notably, there are six aspartate and three glutamate residues in the central channel which are located near positively charged spots and seem to partially compensate for them. This local charge distribution is also consistent with adaptation to a high-salt environment.

The charge distribution observed in the central channel of the halophilic *Hfx*PCNA suggests an interaction mechanism with DNA which seems to be quite different from that at low-salt conditions. It is known that at high salt concentrations the negatively charged DNA phosphate groups as well as the negatively charged amino-acid side chains in proteins are surrounded by cations which can rapidly exchange their positions with other ligands (O'Brien *et al.*, 1998). The increased number of negatively charged Asp and Glu side chains lining the central channel of *Hfx*PCNA can serve as cation-binding sites. During *Hfx*PCNA–DNA interaction the negatively charged DNA phosphate groups would be bound *via* intermediate cations forming bridges to the Asp and Glu side chains (O'Brien *et al.*, 1998; Bergqvist *et al.*, 2003). The central channel of *Hfx*PCNA has a diameter of 36 Å, which is sufficient to accommodate double-stranded DNA (Krishna *et al.*, 1994; Gulbis *et al.*, 1996). In fact, room exists for one or two layers of water between the DNA and PCNA (Johnson & O'Donnell, 2005). Recent molecular-dynamics simulations suggest that the residues lining the PCNA channel interact with the phosphodiester backbone of DNA. However, these interactions are highly dynamic and seem to be frequently displaced by ions from the solution (Ivanov *et al.*, 2006). We assume that in the case of *Hfx*PCNA the bridging cations would favour a similarly dynamic manner of DNA binding. Recent measurements of diffusional properties as a function of viscosity and protein size suggested that PCNA moves along DNA using two different sliding mechanisms: (i) by rotationally tracking the helical pitch or (ii) by sliding uncoupled from the helical pitch (Kochaniak *et al.*, 2009). The observation of only a very weak relation between ionic strength and diffusion properties suggested that PCNA maintains electrostatic contact with the DNA phosphate backbone while moving. In the high-salinity environment of *Hfx*PCNA, screening of the repulsive interactions between Asp and Glu residues and the DNA phosphate backbone by cation bridges could allow a dynamic sliding interaction in a manner analogous to that described above.

The presence of mainly positive charges, as found in *P. furiosus* PCNA and *A. fulgidus* PCNA (Figs. 5*b* and 5*c*), in the DNA-interacting channel of a PCNA functioning at high salt concentration would be likely to lead to strong binding of anions which would unfavourably interfere with the DNA–PCNA interaction. Thus, the presence of a channel lined mainly by negative charges seems to represent an adaptive structural feature of halophilic PCNA molecules allowing binding interactions between two negatively charged binding partners *via* cation bridges.

4. Conclusion

The structure of PCNA from the extremely halophilic archaeon *H. volcanii* has revealed specific features of the protein that are likely to reflect adaptation to a high-salt environment. Our study suggests a different type of interaction with DNA in halophilic PCNAs that is mediated by cation bridges between the phosphodiester groups on DNA and abundant negative charges lining the central channel of PCNA. The ease with which *H. volcanii* can be cultured in the laboratory and the availability of tools for reverse genetic manipulation of this organism will allow these predictions to be tested by mutational analysis *in vivo*.

We thank Thorsten Allers (University of Nottingham, England) for supplying *H. volcanii* DS70, Xiaofeng Zhang for technical assistance during data collection and Malcolm White (University of St Andrews, Scotland) for advice. We gratefully acknowledge the access to synchrotron-radiation facilities at

the ESRF (Grenoble, France) and thank the staff for the help at the beamline. FCG and SM were funded in Copenhagen by Forskningsrådet for Natur og Univers. SM is currently funded by the Scottish Universities Life Sciences Alliance (SULSA).

References

Adams, P. D., Grosse-Kunstleve, R. W., Hung, L.-W., Ioerger, T. R., McCoy, A. J., Moriarty, N. W., Read, R. J., Sacchettini, J. C., Sauter, N. K. & Terwilliger, T. C. (2002). *Acta Cryst.* D**58**, 1948–1954.

Allers, T. & Mevarech, M. (2005). *Nature Rev.* **6**, 58–73.

Bergqvist, S., Williams, M. A., O'Brien, R. & Ladbury, J. E. (2003). *Biochem. Soc. Trans.* **31**, 677–680.

Bourenkov, G. P. & Popov, A. N. (2006). *Acta Cryst.* D**62**, 58–64.

Bowman, G. D., O'Donnell, M. & Kuriyan, J. (2004). *Nature (London)*, **429**, 724–730.

Bruning, J. B. & Shamoo, Y. (2004). *Structure*, **12**, 2209–2219.

Chapados, B. R., Hosfield, D. J., Han, S., Qiu, J., Yelent, B., Shen, B. & Tainer, J. A. (2004). *Cell*, **116**, 39–50.

Collaborative Computational Project, Number 4 (1994). *Acta Cryst.* D**50**, 760–763.

DeLano, W. L. (2002). *The PyMOL Molecular Graphics System.* http://www.pymol.org.

Emsley, P. & Cowtan, K. (2004). *Acta Cryst.* D**60**, 2126–2132.

Gasteiger, E., Hoogland, C., Gattiker, A., Duvaud, S., Wilkins, M. R., Appel, R. D. & Bairoch, A. (2005). *The Proteomics Protocols Handbook*, edited by J. M. Walker, pp. 571–607. Totowa: Humana Press.

Grabowski, B. & Kelman, Z. (2003). *Annu. Rev. Microbiol.* **57**, 487–516.

Gulbis, J. M., Kelman, Z., Hurwitz, J., O'Donnell, M. & Kuriyan, J. (1996). *Cell*, **87**, 297–306.

Hishiki, A., Hashimoto, H., Hanafusa, T., Kamei, K., Ohashi, E., Shimizu, T., Ohmori, H. & Sato, M. (2009). *J. Biol. Chem.* **284**, 10552–10560.

Ivanov, I., Chapados, B. R., McCammon, J. A. & Tainer, J. A. (2006). *Nucleic Acids Res.* **34**, 6023–6033.

Johnson, A. & O'Donnell, M. (2005). *Annu. Rev. Biochem.* **74**, 283–315.

Jones, T. A., Zou, J.-Y., Cowan, S. W. & Kjeldgaard, M. (1991). *Acta Cryst.* A**47**, 110–119.

Karshikoff, A. & Ladenstein, R. (2001). *Trends Biochem. Sci.* **26**, 550–556.

Kochaniak, A. B., Habuchi, S., Loparo, J. J., Chang, D. J., Cimprich, K. A., Walter, J. C. & van Oijen, A. M. (2009). *J. Biol. Chem.* **284**, 17700–17710.

Kontopidis, G., Wu, S. Y., Zheleva, D. I., Taylor, P., McInnes, C., Lane, D. P., Fischer, P. M. & Walkinshaw, M. D. (2005). *Proc. Natl Acad. Sci. USA*, **102**, 1871–1876.

Krishna, T. S., Kong, X. P., Gary, S., Burgers, P. M. & Kuriyan, J. (1994). *Cell*, **79**, 1233–1243.

MacNeill, S. A. (2009). *Biochem. Soc. Trans.* **37**, 108–113.

Matsumiya, S., Ishino, S., Ishino, Y. & Morikawa, K. (2002). *Genes Cells*, **7**, 911–922.

Matsumiya, S., Ishino, Y. & Morikawa, K. (2001). *Protein Sci.* **10**, 17–23.

Mullakhanbhai, M. F. & Larsen, H. (1975). *Arch. Microbiol.* **104**, 207–214.

Muller, V. & Oren, A. (2003). *Extremophiles*, **7**, 261–266.

O'Brien, R., DeDecker, B., Fleming, K. G., Sigler, P. B. & Ladbury, J. E. (1998). *J. Mol. Biol.* **279**, 117–125.

Otwinowski, Z. & Minor, W. (1997). *Methods Enzymol.* **276**, 307–326.

Sakurai, S., Kitano, K., Yamaguchi, H., Hamada, K., Okada, K., Fukuda, K., Uchida, M., Ohtsuka, E., Morioka, H. & Hakoshima, T. (2005). *EMBO J.* **24**, 683–693.

Thompson, J. D., Higgins, D. G. & Gibson, T. J. (1994). *Nucleic Acids Res.* **22**, 4673–4680.

Vijayakumar, S., Chapados, B. R., Schmidt, K. H., Kolodner, R. D., Tainer, J. A. & Tomkinson, A. E. (2007). *Nucleic Acids Res.* **35**, 1624–1637.

Warbrick, E. (1998). *Bioessays*, **20**, 195–199.

Wendoloski, D., Ferrer, C. & Dyall-Smith, M. L. (2001). *Microbiology*, **147**, 959–964.

Williams, G. J., Johnson, K., Rudolf, J., McMahon, S. A., Carter, L., Oke, M., Liu, H., Taylor, G. L., White, M. F. & Naismith, J. H. (2006). *Acta Cryst.* F**62**, 944–948.

Xing, G., Kirouac, K., Shin, Y. J., Bell, S. D. & Ling, H. (2009). *Mol. Microbiol.* **71**, 678–691.

Yeates, T. O. (1997). *Methods Enzymol.* **276**, 344–358.